Resonant probing spin-0 and spin-2 dark matter mediators with fixed target experiments

I. V. Voronchikhin[1,*] and D. V. Kirpichnikov[2,†]
[1]*Tomsk Polytechnic University, 634050 Tomsk, Russia*
[2]*Institute for Nuclear Research, 117312 Moscow, Russia*

(Received 28 April 2023; accepted 15 June 2023; published 29 June 2023)

We discuss the mechanism to produce electron-specific dark matter mediators of spin-0 and spin-2 in the electron fixed target experiments such as NA64 and LDMX. The secondary positrons induced by the electromagnetic shower can produce the mediators via annihilation on atomic electrons. That mechanism, for some selected kinematics, results in the enhanced sensitivity with respect to the bounds derived by the bremsstrahlunglike emission of the mediator in the specific parameter space. We derive the corresponding experimental reach of the NA64 and LDMX.

DOI: 10.1103/PhysRevD.107.115034

I. INTRODUCTION

The fundamental particle content of the Dark Matter (DM) can not be explained by the Standard Model (SM) even though it is associated with nearly ≃85% matter of the Universe [1,2]. The indirect manifestations of the DM are related mainly to the galaxy rotation velocities, large-scale structures, the cosmic microwave background anisotropy, the gravitational lensing, etc., [3–5]. However, the direct detection of the DM particles remains one of the most significant challenges of fundamental physics.

One can assume the thermal origin of the DM, implying the equilibrium between the DM and visible matter in the early Universe [6]. In order to avoid the DM overproduction through thermal freeze-out, an idea of existence of the light massive mediator (MED) of DM has been introduced [7–12]. For instance, the typical scenarios with dark boson mediators include spin-0, spin-1, and spin-2 particles such as the hidden Higgs boson [13–19], the dark photon [20–32], and dark graviton [33–45], respectively. Note that, the fermion DM portals have also recently been discussed in the literature [46–51]. The various mechanisms of DM thermalization involving mediators were studied by the authors of Refs. [52–57]. For recent review of the probing these scenarios with accelerator-based experiments, see the Refs. [58–66] and references therein.

In this paper we focus on resonant probing the electron-specific spin-0 (spin-2) DM mediator, denoted by $\phi(G)$, with electron fixed target experiments, such as NA64 [67–89] and LDMX [12,90–97]. The typical production mechanisms of spin-0 (spin-2) DM mediator in the reaction of high-energy electrons on a fixed target are associated with $\phi(G)$-strahlung in nucleus scattering, $e^-N \to e^-N\phi(G)$, and resonant annihilation of secondary positrons on atomic electrons, $e^+e^- \to \phi(G)$. In the present paper we consider mostly the invisible decay channels of mediators into pairs of specific DM particles, $\phi(G) \to \mathrm{DM} + \mathrm{DM}$.

It is worth mentioning that all DM benchmark scenarios of the present paper imply the light m_{DM} to be in the range 1 MeV–1 GeV, such that these masses could be well within experimental reach of the current and forthcoming accelerator-based facilities. Furthermore, these direct DM production limits are complementary to the DM relic-density parameter space [12,34].

In addition, we note that for both NA64 and LDMX experimental facilities, the resonant production of A' spin-1 DM mediator, $e^+e^- \to A' \to \mathrm{DM} + \mathrm{DM}$, has been studied explicitly in Refs. [83,84,96–100]. It was shown that including the annihilation channel can provide the improved bounds on thermal DM parameter space. Therefore, the resonant probing spin-0 and spin-2 DM mediators can extend the experimental reach of NA64e and LDMX, filling a gap in the existing literature [12,80,87].

This paper is organized as follows. In Sec. II we discuss the benchmark scenarios for the electron-specific DM mediators of spin-2 and spin-0. In Sec. III we provide a description of existing expressions for the double differential cross section of MED for the electron bremsstrahlung-like process in the case of Weizsäcker-Williams (WW) approach. In this section we also derive explicitly the resonant mediator production cross sections and its decay

*Corresponding author.
i.v.voronchikhin@gmail.com
†dmbrick@gmail.com

of widths into DM. In Sec. IV we briefly discuss the main aspects of the positron track length distribution. In Sec. V we discuss the missing energy signal and overview the main benchmark parameters of the electron fixed target facilities. In Sec. VI we study the typical ranges of MED mass that yield the resonant enhancement of the MED parameter space. In Sec. VII we obtain the experimental reach of NA64 and LDMX for spin-2 and spin-0 MED. We conclude in Sec. VIII.

II. BENCHMARK SCENARIOS

A. Tensor DM mediator

Let us consider first the benchmark simplified coupling between the SM particles and the massive spin-2 field $G_{\mu\nu}$ that is described by the following electron-specific effective Lagrangian [33,34],

$$\mathcal{L}^{\rm G}_{\rm eff} \supset -\frac{ic^{\rm G}_{ee}}{2\Lambda} G^{\mu\nu}(\bar{e}\gamma_\mu \overleftrightarrow{D}_\nu e - \eta_{\mu\nu}\bar{e}\gamma_\rho \overleftrightarrow{D}^\rho e) + \frac{c^{\rm G}_{\gamma\gamma}}{\Lambda} G^{\mu\nu}\left(\frac{1}{4}\eta_{\mu\nu}F_{\lambda\rho}F^{\lambda\rho} + F_{\mu\lambda}F^{\lambda}_{\nu}\right) + \frac{c^{\rm G}_{\rm DM}}{\Lambda} G^{\mu\nu}T^{\rm DM}_{\mu\nu}, \tag{1}$$

where e is the label of the SM electron, $F_{\mu\nu} = \partial_\mu A_\nu - \partial_\nu A_\mu$ is a stress tensor of the SM photon field A_μ, $D_\mu = \partial_\mu - ieA_\mu$ is a covariant derivative of the $U(1)$ gauge field, and Λ is the dimensional parameter for spin-2 interactions, that is associated with the scale of new physics; $c^{\rm G}_{ee}$ and $c^{\rm G}_{\gamma\gamma}$ are dimensionless couplings for the electron and photon respectively. We choose the universal coupling $c^{\rm G}_{ee} = c^{\rm G}_{\gamma\gamma}$ throughout the paper, in order to protect the unitarity of the scenario at low energies (see e.g., Ref. [34] and references therein for detail). In addition, to be more concrete, for the model with massive tensor mediator, $G_{\mu\nu}$, the DM candidates are chosen to be either a light Dirac fermion ψ or hidden massive scalar S, such that the energy-momentum tensor $T^{\rm DM}_{\mu\nu}$ in Eq. (1) is given, respectively, by [34]

$$T^{S}_{\mu\nu} = \partial_\mu S \partial_\nu S - \frac{1}{2}\eta_{\mu\nu}(\partial_\rho S)^2 - \frac{1}{2}\eta_{\mu\nu}m_S^2 S^2, \tag{2}$$

$$T^{\psi}_{\mu\nu} = \frac{i}{4}[\bar{\psi}(\gamma_\mu\partial_\nu + \gamma_\nu\partial_\mu)\psi - (\partial_\mu\bar{\psi}\gamma_\nu + \partial_\nu\bar{\psi}\gamma_\mu)] - \eta_{\mu\nu}(\bar{\psi}\gamma^\rho\partial_\rho\psi - m_\psi\bar{\psi}\psi), \tag{3}$$

where m_S and m_ψ are the masses of S and ψ, respectively. It is worth mentioning that the specific coupling constants $c^{\rm G}_{\rm DM} = (c^{\rm G}_{SS}, c^{\rm G}_{\psi\psi})$ in Eq. (1) and the set of masses $m_{\rm DM} = (m_S, m_\psi)$ are assumed to be independent throughout the paper.

B. Scalar mediator

Let us consider now the electron-specific interaction with a light scalar DM mediator in the following form [12]:

$$\mathcal{L}^{\phi}_{\rm eff} \supset c^{\phi}_{ee}\phi\bar{e}e,$$

where c^{ϕ}_{ee} is the dimensionless coupling of electron with ϕ. The low-energy Lagrangian can arise through flavor-specific five-dimensional effective operator [12,26,101–103]

$$\mathcal{L}_{\rm dim\,5} \supset \sum_{i=e,\mu,\tau}\left[\frac{c_i}{\Lambda}\phi\bar{E}^i_L H e^i_R + \text{H.c.}\right],$$

with c_i being a Wilson coefficient for a flavor index $i = (e,\mu,\tau)$, H, E^i_L, and e^i_R are the SM Higgs doublet, lepton doublet, and lepton singlet, respectively. As emphasized in Ref. [12,26] one can choose the coupling of ϕ predominantly to one flavor in order to avoid dangerous lepton flavor-violating currents, such that $c_e \neq 0$ and $c_\mu \equiv c_\tau \equiv 0$. Note that various ultraviolet completions of that scenario have been suggested already, i.e., in two-Higgs-doublet models involving extra-scalar singlet or vectorlike quarks [26,104,105].

Next, to be more specific, for the scenario with electrophilic scalar mediator ϕ we choose Majorana fermion as well motivated DM candidate [12]. The effective Lagrangian reads as follows [12,106]:

$$\mathcal{L}^{\phi}_{\rm Majorana} \supset -\frac{1}{2}c^{\phi}_{\chi\chi}\phi\chi\chi + \frac{1}{2}m_\chi\chi\chi + \text{H.c.}, \tag{4}$$

where $c^{\phi}_{\chi\chi}$ is the real dimensionless coupling, χ is a two component neutral Majorana DM and m_χ is its mass. The latter implies two on shell real degrees of freedom for χ as soon as $m_\chi \neq 0$.

III. CROSS SECTION

A. Bremsstrahlunglike production of mediator

In this subsection, we consider the double differential cross section for a bremsstrahlung-like production of MED of spin-0 and spin-2 by exploiting the WW approximation [see e.g., Fig. 1(a) and 1(b) for detail]. This approach can be used for the approximation of the exact tree-level production cross sections at the level of $\lesssim 2\%$ for both hidden spin-0 and spin-1 bosons [107–110].

The typical bremsstrahlung-like process in a case of electron primary beam reads as

$$e^-(p) + N(P_i) \to e^-(p') + N(P_f) + \text{MED}(k), \tag{5}$$

where $p = (E_0, \boldsymbol{p})$, $p' = (E'_0, \boldsymbol{p}')$ are the momenta of incoming and outgoing electrons, respectively, $k = (E_{MED}, \boldsymbol{k})$ is the momentum of MED, $P_i = (M, 0)$ and

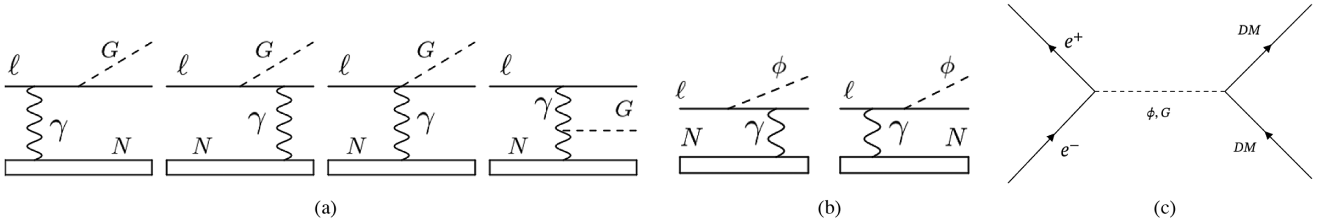

FIG. 1. Feynman diagrams describing production of G- (a) and ϕ- (b) mediators via the bremsstrahlung missing energy process $eN \to eNG$ and $eN \to eN\phi$, respectively. The diagram (c) describes s-channel production of scalar and tensor DM mediators decaying resonantly into specific types of DM particles; $e^+e^- \to \phi \to \chi\chi$ and $e^+e^- \to G \to \psi\bar{\psi}(SS)$.

$P_f = (P_f^0, \boldsymbol{P}_f)$ are the momenta of the initial and outgoing nucleus, respectively, $P_i - P_f = q$, where $q = (q_0, \boldsymbol{q})$ is the four-momentum of transfer to nucleus, we define $t \equiv -q^2$ throughout the paper. Also, the Mandelstam variables take the following form:

$$s_2 = (p+q)^2, \qquad u_2 = (p-k)^2, \qquad t_2 = (p-p')^2. \quad (6)$$

For the production of spin-2 MED in a process (5), the double differential cross section for the approach $m_e/m_G \ll 1$ is given by the following expression [87]:

$$\left.\frac{d\sigma(p+P_i \to p'+P_f+k)}{dx\,d\cos(\theta_G)}\right|_{WW} = -\frac{\alpha\chi}{\pi}\frac{E_{e^-}^2 x\beta_G}{1-x}\frac{1}{8\pi s_2^2} \times 4\pi\alpha\frac{(c_{ee}^{\mathrm{G}})^2}{\Lambda^2}\frac{[(t_2+u_2)^2+(u_2-m_G^2)^2][4u_2s_2+m_G^2t_2]}{4t_2u_2s_2}, \quad (7)$$

where $\alpha = e^2/(4\pi) \simeq 1/137$ is the fine structure constant, $x = E_G/E_0$ is the energy fraction that spin-2 MED carries away, θ_G is the angle between the initial lepton direction and the momentum of the produced G-boson and $\beta_G = \sqrt{1-m_G^2/(xE_0)^2}$ is the typical velocity of G-boson. The flux of virtual photon χ from nucleus is expressed through Tsai's elastic form-factor as follows [111–114]:

$$\chi = Z^2\int_{t_{\min}}^{t_{\max}}\frac{t-t_{\min}}{t^2}\left(\frac{t}{(t_a+t)}\frac{1}{(1+t/t_d)}\right)^2 dt, \quad (8)$$

where $\sqrt{t_a} = 1/R_a$ is a momentum transfer associated with nucleus Coulomb field screening due to the atomic electrons, with R_a being a typical magnitude of the atomic radius $R_a = 111Z^{-1/3}/m_e$, $\sqrt{t_d} = 1/R_n$ is the typical momentum associated with nuclear radius R_n, such that $R_n \simeq 1/\sqrt{d}$ and $d = 0.164A^{-2/3}$ GeV^2. We also note that each Mandelstam variable in Eqs. (6) and (8) is a function of E_{e-}, m_G x and θ_G in the WW approach, the explicit expressions for these functions (i. e. for s_2, u_2, t_2, $t_{\min}$ and $t_{\max}$) are given in Ref. [87].

Also, for a similar ϕ-strahlung process with assuming $m_e/m_\phi \ll 1$ the differential cross section takes the following form [107]:

$$\left.\frac{d\sigma(p+P_i \to p'+P_f+k)}{dx\,d\cos(\theta_\phi)}\right|_{WW} = \frac{\alpha\chi}{\pi}\frac{E_{e^-}^2 x\beta_\phi}{1-x}\frac{4\pi\alpha(c_{ee}^{\phi})^2}{8\pi s_2^2} \times\left(\frac{x^2}{1-x}+2m_\phi^2\frac{u_2x+m_\phi^2(1-x)}{u_2^2}\right), \quad (9)$$

where $x = E_\phi/E_0$ is the energy fraction that is carried away by the spin-0 mediator, θ_ϕ is the angle between the initial electron direction and the momentum of the produced ϕ-boson and $\beta_\phi = \sqrt{1-m_\phi^2/(xE_0)^2}$ is the typical velocity of spin-0 boson.

It is worth mentioning that for a calculation of flux of virtual photons one can use such form-factors as Helm or exponential [115–118]. However, for the mass range of interest $m_{\mathrm{MED}} \lesssim 1$ GeV, the exploiting of these form factors does not provide a sizable impact on the magnitude of the virtual photon flux [87].

B. The resonant production mechanism

In this subsection, for the benchmark scenarios considered in Sec. II, we discuss the production cross section of the $\phi(G)$-boson that is associated with the annihilation of the secondary positrons with atomic electrons [see e.g., Fig. 1(c) for detail].

The first key ingredient for the annihilation cross-section calculation is the partial decay width of hidden bosons. For the case of the spin-2 boson the decay widths into pairs of light scalars, dark fermions, and a electron-positron pair read, respectively, as follows [33]:

$$\Gamma_{G\to\psi\bar{\psi}} = \frac{4\pi\alpha_\psi m_G^3}{160\pi}\left(1+\frac{8}{3}\frac{m_\psi^2}{m_G^2}\right)\left(1-4\frac{m_\psi^2}{m_G^2}\right)^{3/2}, \quad (10)$$

$$\Gamma_{G\to SS} = \frac{4\pi\alpha_S m_G^3}{960\pi}\left(1-4\frac{m_S^2}{m_G^2}\right)^{5/2}, \quad (11)$$

$$\Gamma_{G\to e^+e^-} \simeq \frac{(c_{ee}^{\rm G}/\Lambda)^2 m_G^3}{160\pi}, \tag{12}$$

where we denote the dimensional dark-fine structure constants as $\alpha_\psi = (c_{\psi\psi}^{\rm G})^2/(4\pi\Lambda^2)$ and $\alpha_S = (c_{SS}^{\rm G})^2/(4\pi\Lambda^2)$, we also imply that $m_e/m_G \ll 1$. The resonant total cross section for spin-2 MED for the case of Dirac DM is

$$\sigma_{e^-e^+\to G\to\psi\bar\psi} = \frac{4\pi\alpha_\psi (c_{ee}^{\rm G})^2}{256\pi\Lambda^2} \frac{s^3}{(s-m_G^2)^2 + m_G^2(\Gamma_G^{\rm tot})^2} \times (1+8m_\psi^2/(3s))(1-4m_\psi^2/s)^{3/2}, \tag{13}$$

where $s = (p_{e_-} + p_{e_+})^2$ is Mandelstam variable, p_{e_-} and p_{e_+} are the typical 4-momenta of the atomic electrons and secondary positrons, respectively. In the case of scalar DM the cross section takes following form:

$$\sigma_{e^-e^+\to G\to SS} = \frac{4\pi\alpha_S (c_{ee}^{\rm G})^2}{1536\pi\Lambda^2} \frac{s^3(1-4m_S^2/s)^{5/2}}{(s-m_G^2)^2 + m_G^2(\Gamma_G^{\rm tot})^2}. \tag{14}$$

For the calculation of both the decay width and cross section associated with spin-2 mediator we implement Feynman rules from Ref. [33] into the state-of-the-art FeynCalc package [119,120] for the Wolfram Mathematica routine [121]. In addition, we reproduce the well-known results for the massive graviton decay widths [33].

Next, the widths of the decay of the scalar MED into both the Majorana DM and electron-positron pair read, respectively, as follows:

$$\Gamma_{\phi\to\chi\chi} = \frac{1}{2}\cdot\frac{4\pi\alpha_\chi m_\phi}{8\pi}\left(1-4\frac{m_\chi^2}{m_\phi^2}\right)^{3/2}, \tag{15}$$

$$\Gamma_{\phi\to e^+e^-} \simeq \frac{(c_{ee}^{\phi})^2 m_\phi}{8\pi}, \tag{16}$$

where $\alpha_\chi = (c_{\chi\chi}^{\phi})^2/(4\pi)$ is a dimensionless dark-fine structure constant.

Finally, the resonant total cross section in the case of scalar MED and Majorana DM reads as

$$\sigma_{e^+e^-\to\phi\to\chi\chi} = \frac{1}{2}\cdot\frac{4\pi\alpha_\chi (c_{ee}^{\phi})^2}{16\pi} \frac{s(1-4m_\chi^2/s)^{3/2}}{(s-m_\phi^2)^2 + m_\phi^2(\Gamma_\phi^{\rm tot})^2}. \tag{17}$$

The derivation of the decay width (15) and cross section (17) with Majorana particles in the final state is carried out in Appendix. It is important to emphasize that the total phase space for the 2-component Majorana spinors should be multiplied by the additional factor of $1/2$ in order to take into account the identical neutral particles χ (see e.g., Ref. [122] and references therein for detail). Therefore, the well-known the result for the cross section with Dirac fermions ψ_D in the final state [11] can be reproduced from Eq. (17) if one omits its prefactor $1/2$. The latter cross-check can be also carried out for the decay width of scalar into Majorana particles Eq. (15). That implies the typical Lagrangian terms for the Dirac 4-components fermion

$$\mathcal{L}_{\rm Dirac}^{\phi} \supset c_{\psi_D\psi_D}^{\phi}\phi\bar\psi_D\psi_D + m_{\psi_D}\bar\psi_D\psi_D,$$

and the replacement $c_{\chi\chi}^{\phi} \to c_{\psi_D\psi_D}^{\phi}$ and $m_\chi \to m_{\psi_D}$ in Eqs. (15) and (17) [compare it with Eq. (4) for clarification].

In the present study, we focus on the invisible decay mode of the mediators, which means that $m_{\rm MED} \gtrsim 2m_{\rm DM}$ and $\Gamma_{\rm MED\to e^+e^-} \ll \Gamma_{\rm MED\to DM\,DM}$ throughout the paper. This implies three benchmark decay widths

$$\Gamma_G^{\rm tot} \simeq \Gamma_{G\to\psi\bar\psi}, \qquad \Gamma_G^{\rm tot} \simeq \Gamma_{G\to SS}, \qquad \Gamma_\phi^{\rm tot} \simeq \Gamma_{\phi\to\chi\chi},$$

for the analysis of the electron missing energies signatures associated with accelerator based experiments NA64 and LDMX. Therefore, it leads to the rapid decay of the mediator into a pair of DM after its production.

IV. POSITRON TRACK-LENGTH DISTRIBUTION

In this section we briefly discuss the distribution of positrons in a target due to the electromagnetic shower development from the incoming primary electron (positron) beams.

The analytical approximations for the typical positron track-length distribution $T(E_{e^+})$ were studied in detail [98,123–126]. For the thick target it was shown that $T(E_{e^+})$ depends, at first order, on a specific type of target material through the multiplicative factor $T(E_{e^+}) \propto X_0$, that corresponds to the radiation length [X_0 is a typical distance over which a high-energy electron (positron) loses all but $1/e$ of its energy due to the bremsstrahlung, $e^\pm N \to e^\pm N\gamma$, where $e \simeq 2.71828$ is a Euler's number]. Moreover, $T(E_{e^+})$ depends also on the ratio E_{e^+}/E_0, where E_0 is the energy of the primary impinging particle that initiates electromagnetic shower development in the thick target (see e.g., Fig. 2 for detail), so that one can exploit the typical distribution shown in Fig. 2 for the specific type of electron fixed target experiment that is characterized by energy of primary beam E_0 and target material X_0. The distribution in Fig. 2 is adapted [127] from Refs. [83,84], that implies numerical Monte Carlo simulations for the electromagnetic (EM) shower development in GEANT4 [128].

To conclude this section we note that a positron track length depends also on the typical angles between the primary beam direction and momentum of the secondary positrons. However, this dependence impacts on the electromagnetic shower development at the level of $\lesssim\mathcal{O}(1\%)$ and hence the angular effects can be safely neglected in the estimates [98].

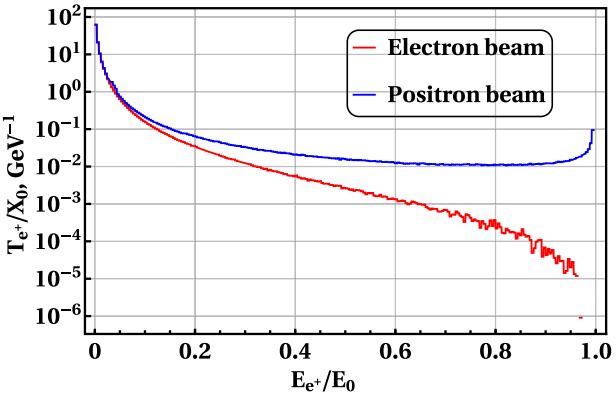

FIG. 2. The differential positron track-length distribution as function of ratio between the secondary positron energy E_{e^+} and a primary beam energy E_0 of the electron (red line) or positron (blue line).

V. MISSING ENERGY SIGNAL

In this section we discuss the electron missing energy signatures and the typical parameters of the NA64 and LDMX experiments for probing DM mediators. It is worth mentioning that both NA64e and LDMX experiments have background suppression at the level of $\lesssim\mathcal{O}(10^{-13}$–$10^{-12})$.

We estimate the number of MEDs produced due to the bremsstrahlung for fixed target facilities as follows:

$$N^{\rm brem}_{\rm MED} \simeq {\rm EOT}\cdot\frac{\rho N_A}{A}L_T\int_{x_{\rm min}}^{x_{\rm max}}dx\frac{d\sigma_{2\to3}(E_0)}{dx}\eta^{\rm brem}_{\rm MED}, \tag{18}$$

where L_T is effective interaction length of the electron in the target, EOT is number of electrons accumulated on target, ρ is target density, N_A is Avogadro's number, A is the atomic weight number, Z is the atomic number, $\eta^{\rm brem}_{\rm MED}$ is a typical efficiency for the bremsstrahlung emission of the MED, $d\sigma_{2\to3}/dx$ is the differential cross section of the electron-missing energy process $eN\to eN\phi(G)$, $E_0\equiv E_{\rm beam}$ is the initial energy of electron beam, and $x_{\rm min}$ and $x_{\rm max}$ are the minimal and maximal fraction of missing energy, respectively for the experimental setup, $x\equiv E_{miss}/E_0$, where $E_{\rm miss}\equiv E_{\rm MED}$. The $x_{\rm min}\lesssim x\lesssim x_{\rm max}$ cut is determined by specific fixed-target facility.

The typical number of hidden bosons produced due to the annihilation is estimated to be [84,98]

$$N^{\rm ann}_{\rm MED} \simeq {\rm EOT}\frac{\rho N_A Z L_T}{A}\int_{E^{\rm cut}_{e^+}}^{E^{\rm max}_{e^+}}dE_{e^+}\sigma_{\rm tot}(E_{e^+})T(E_{e^+})\eta^{\rm ann}_{\rm MED}, \tag{19}$$

where $\sigma_{\rm tot}(E_{e^+})$ is the resonant total cross section of the electron-positron annihilation into DM, $\eta^{\rm ann}_{\rm MED}$ is a typical efficiency associated with MED production via the resonant channel (we conservatively imply throughout the paper that signals for both positron and electron beam modes have the same efficiency $\eta^{\rm ann}_{\rm MED}$), E_{e^+} is the energy of secondary positrons, $E^{\rm cut}_{e^+}=E_0x_{\rm min}$ and $E^{\rm max}_{e^+}=E_0$ are the minimal and maximal energies of secondary positrons in the EW shower, respectively.

NA64e: the NA64e is the fixed target experiment located at CERN North Area with a beam from the Super Proton Synchrotron (SPS) H4 beamline. The ultrarelativistic electrons (positrons) of $E_0\simeq 100$ GeV can be exploited as the primary beam that is scattering off nuclei of an active thick target. The typical scheme of the NA64 setup can be found elsewhere in Ref. [84].

The detector is equipped with: (i) a low-material-budget tracker allowing the measurement of initial beam momentum with the precision of 1%; (ii) two magnetic spectrometers deflecting the primary beam line; (iii) synchrotron radiation detector (SRD) that is used for the suppression of hadron beam contamination and the effective tagging of the charged particles via their synchrotron radiation (SR); (iv) the active target represents electromagnetic calorimeter (ECAL) that is Shashlik-type modules consisting of alternating plastic scintillator (Sc) and lead absorber (Pb).

The fraction of the primary beam energy $E_{\rm miss}=xE_0$ can be carried away by DM pair, that passes the NA64e detector without energy deposition. The remaining part of the beam energy fraction, $E^{\rm rec}_e\simeq(1-x)E_0$, can be deposited in the electromagnetic calorimeter (ECAL) of NA64e by the recoil electrons (positrons). For the NA64e experiment we use the following benchmark parameters ($\rho\simeq 11.34$ g cm^{-3}, $A=207$ g mole^{-1}, $Z=82$, $X_0=2.56$ cm), the effective interaction length of the electron is $L_T=X_0$ and the missing energy fraction cut is $x_{\rm min}=0.5$. The efficiencies $\eta^{\rm brem}_{\rm MED}$ and $\eta^{\rm ann}_{\rm MED}$ are taken to be at the level of 90% for both electron and positron beam modes [84].

The event selection rule for NA64e can be summarized as follows [129]:

(1) the beam track momentum should be within 100 ± 3 GeV;
(2) the energy detected by the SRD should be consistent with the SR energy emitted by $e^{\pm}$'s in the magnets of the spectrometer;
(3) the shower shape in the ECAL should be as expected from the signal-event shower [67] implying the cut for the recoil electron (positron) $E^{\rm rec}_e\lesssim 0.5E_0\simeq 50$ GeV.

We note that about $\simeq$120 days are needed to collect EOT $\simeq 5\times10^{12}$ at the $H4$ beam line for the projected statistics of the NA64e. In this work we also perform the analysis of the sensitivity of NA64e to probe DM for the EOT $\simeq 3.22\times10^{11}$ (see e.g., Ref. [129] for detail).

The light dark matter experiment (LDMX) is the projected electron fixed-target facility at Fermilab, that can be used for investigating the relic DM with the mass lying in the range between 1 MeV and 1 GeV. The schematic layout of the LDMX experiment is given in Ref. [12]. The projected LDMX facility would employ the aluminium target (Al) and the unique electron missing-momentum

technique [90] that is complementary to the NA64e facility. The missing momentum of the incoming beam can be measured by (i) the beam tagger, (ii) target, (iii) silicon tracker system, and (iv) electromagnetic and hadron calorimeter which are located downstream. Thus, for the LDMX experiment we use the following benchmark parameters ($\rho = 2.7\ \mathrm{g\,cm^{-3}}$, $A = 27\ \mathrm{g\,mole^{-1}}$, $Z = 13$, $X_0 = 8.9$ cm) and $L_T \simeq 0.4X_0 \simeq 3.56$ cm. The typical efficiencies $\eta^{\mathrm{brem}}_{\mathrm{MED}}$ and $\eta^{ann}_{\mathrm{MED}}$ are estimated to be at the level of $\simeq$50% for both electron [91] and positron beam options.

The energy of the primary beam is chosen to be $E_0 \simeq 16$ GeV and the projected moderate statistics corresponds to EOT $\simeq 10^{15}$ (it is planned however to collect EOT $\simeq 10^{16}$ by the final phase of experimental running after 2027, see e.g., Ref. [91] and references therein for detail). The rules for the missing momentum event selection in the LDMX are [12]

(1) the beam track momentum should be measured by the tagger at the level of $\simeq$16 GeV,
(2) the silicon tracker installed downstream the target should tag the large transfer momentum of the recoil particle $e^{\pm}$, that is associated with DM emission,
(3) the shower shape in the ECAL should be as expected from the signal-event shower [12] implying the cut for the recoil electron (positron) $E^{\mathrm{rec}}_e \lesssim 0.3E_0 \simeq 4.8$ GeV.

The explicit study on the background event estimate is provided in Ref. [130] for the electron-bremsstrahlung beam mode only. We rely on that analysis and conservatively expect that for the positron beam mode of LDMX and the annihilation channel the background rejection would be the same.

VI. TYPICAL THRESHOLDS

Let us consider now the kinematics of the above mentioned process in detail. As we discussed earlier, in case of fixed-target experiments, the process of the electron-positron annihilation arises form the interaction of secondary positrons from the EM shower with atomic electrons in the thick active target. The EM shower originates from the primary electron beam impinging on the fixed dump. We neglect the velocity of the atomic electron, therefore the typical momenta of the electrons and secondary positrons are chosen to be $p_{e^-} = (m_e, 0, 0, 0)$ and $p_{e^+} \simeq (E_{e^+}, 0, 0, E_{e^+})$, respectively. Thus, the Mandelstam variable takes the following form:

$$s = (m_e + E_{e^+})^2 - |\boldsymbol{p}_{e^+}|^2 = m_e^2 + 2m_e E_{e^+} \simeq 2m_e E_{e^+}, \quad (20)$$

where we imply that positrons are ultrarelativistic and hence $|\boldsymbol{p}_{e^+}| \simeq E_{e^+}$.

In Fig. 3 for the illustrative purpose we show the resonant total cross sections [see e.g., Eqs. (13) and (17) for detail] as a function of energy fraction between secondary positrons and primary beam for the NA64e experiment.

One can conclude from Fig. 3, that the larger coupling of the mediator to DM, the large total cross section at the peak position in the case of invisible mode Br(MED $\to$ DM DM) $\simeq 1$. However, the position of the peak is related to the m_{MED} and does not dependent on the typical magnitude of dark fine structure constant. The contribution to the total cross section of the process $e^+e^- \to$ MED $\to$ DM DM is associated with the off shell mediator energy range $2m_{\mathrm{DM}} \lesssim \sqrt{s} \lesssim m_{\mathrm{MED}}$, and the typical resonant masses at $m_{\mathrm{MED}} \simeq \sqrt{2m_e E_{e^+}}$. As a result, one can estimate the mass

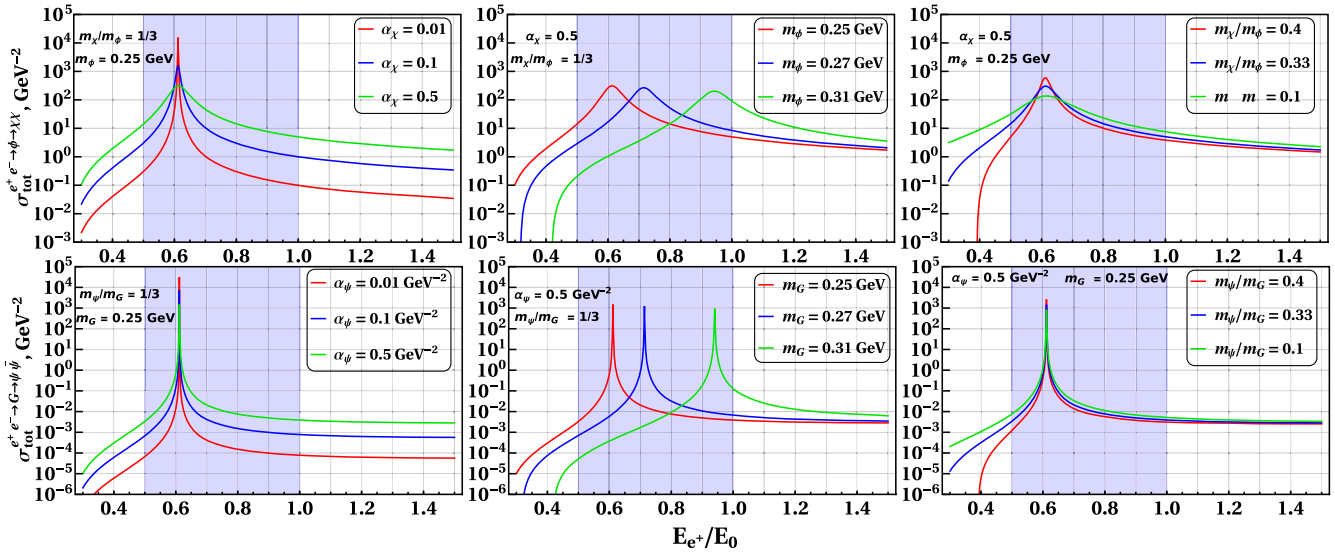

FIG. 3. The resonant total cross section for a scalar mediator (17) (upper panels) and for a tensor mediator (13) (bottom panels) as the function of ratio between positron energy and energy primary beam for the set of coupling constants and masses. For the spin-2 and spin-0 cross sections we set $c^{\mathrm{G}}_{ee}/\Lambda = 1\ \mathrm{GeV}^{-1}$ and $c^{\phi}_{ee} = 1$, respectively. The blue-shaded region corresponds to the typical parameters space associated with the missing energy cuts $0.5 \lesssim E_{e^+}/E_0 \lesssim 1$ of NA64e for $E_0 = 100$ GeV.

range $m_{\rm MED}$ that would enhance the signal in the NA64 due to the MED emission. In particular, the energy deposition cut for NA64e annihilation mode, $E_0/2 \lesssim E_{e^+} \lesssim E_0$, yields the following mass range, $\sqrt{E_0 m_e} \lesssim m_{\rm MED} \lesssim \sqrt{2E_0 m_e}$, that numerically corresponds to the typical signal mass bounds $0.23\ {\rm GeV} \lesssim m_{\rm MED} \lesssim 0.32\ {\rm GeV}$ for $E_0 \simeq 100$ GeV.

It is worth noticing that in the case of LDMX experiment, the shape of the annihilation cross section would be the same, however the typical resonant mass range shifts to the $0.11\ {\rm GeV} \lesssim m_{\rm MED} \lesssim 0.13\ {\rm GeV}$ which implies the missing energy cut $0.7E_0 \lesssim E_{e^+} \lesssim E_0$ for $E_0 \simeq 16$ GeV. It turns out, that the resonant mass range of NA64e is ≃4.48 times wider than the one for the LDMX facility.

One can estimate the typical width of the cross section peak at the resonant point $E_R \simeq m^2_{\rm MED}/(2m_e)$ in terms of positron energy E_{e^+} for the NA64e facility. The latter is crucial for the extraction of the signal yield in the narrow energy region. In particular, by solving the algebraic equation for the Breit-Wigner term in the denominator $((s - m^2_{\rm MED})^2 \simeq m^2_{\rm MED}\Gamma^2_{\rm MED}$ one finds

$$E_\pm \simeq E_R \pm \Delta E/2,$$

where $\Delta E \simeq m_{\rm MED}\Gamma_{\rm MED}/m_e$. In the case of $0.23\ {\rm GeV} \lesssim m_{\rm MED} \lesssim 0.32$ GeV, the range of energy width corresponds to $0.037\ {\rm GeV} \lesssim \Delta E_{e^+} \lesssim 0.14$ GeV for Dirac DM, $\alpha_\psi \simeq 0.5\ {\rm GeV}^{-2}$ and $m_\psi/m_G \simeq 1/3$.

Note that for the scalar DM the energy width is fairly narrow and can be in the range $0.0026\ {\rm GeV} \lesssim \Delta E_{e^+} \lesssim 0.0098$ GeV for $\alpha_S \simeq 0.5\ {\rm GeV}^{-2}$ and $m_S/m_G \simeq 1/3$. Finally, for the typical resonant mass range of the LDMX facility $0.11\ {\rm GeV} \lesssim m_\phi \lesssim 0.13$ GeV the positron energy resolution can be relatively large $1.22\ {\rm GeV} \lesssim \Delta E_{e^+} \lesssim 1.71$ GeV for $\alpha_\chi \simeq 0.5$ and $m_\chi/m_\phi \simeq 1/3$.

One can estimate the on shell mediator production cross section for the narrow-width regime as long as $\Gamma_{\rm MED} \to 0$ in the following form:

$$\sigma_{e^-e^+\to G\to\psi\bar\psi} = \sigma_{e^-e^+\to G\to SS} = \delta(s - m_G^2)\tilde c_G, \quad (21)$$

$$\sigma_{e^-e^+\to\phi\to\chi\chi} = \delta(s - m_G^2)\tilde c_\phi, \quad (22)$$

where the dimensionless normalization prefactors read as follows:

$$\tilde c_G = 5\pi(c^G_{ee})^2 m_G^2/(8\Lambda^2), \qquad \tilde c_\phi = \pi(c^\phi_{ee})^2/2. \quad (23)$$

In Eqs. (21) and (22) we use the representation of Dirac delta function,

$$\delta(x) = \lim_{\Gamma\to 0}\Gamma/[\pi(x^2 + \Gamma^2)].$$

It follows from Eqs. (21)–(23) that at the first order the resonant total cross section does not depend on the coupling between the DM and MED [83]. Moreover, for the spin-2 mediator the cross section is agnostic to the specific type of the outgoing DM particles.

By taking into account that a dominant contribution to the resonant cross section is close to $s \simeq m^2_{\rm MED}$ for the near-threshold approach $m_{\rm MED} \simeq 2m_{\rm DM}$ ($\Gamma_{\rm MED} \to 0$) we get the signal yield for the resonant process in the following form:

$$N^{\rm ann}_{\rm MED} = {\rm EOT} \times \frac{N_A Z L_T \rho}{A}\frac{\tilde c_{\rm MED} T_+(E_R)}{2m_e} \times \theta(E_R - E^{\rm cut}_{e^+})\theta(E^{\rm max}_{e^+} - E_R), \quad (24)$$

where $\tilde c_{\rm MED}$ is defined by Eq. (23), $E_R = m^2_{\rm MED}/(2m_e)$ is the typical energy of the resonance, $\theta(x)$ is the Heaviside step function.

VII. THE EXPERIMENTAL LIMITS

In this section we study the experimental reach of fixed-target facilities NA64e and LDMX for both primary electron and positron beams for spin-2 and spin-0 DM assuming their invisible decay mode. For the background-free case and the null results of the missing energy events associated with DM mediator production, we set the number of signal events $N_{\rm sign} \gtrsim 2.3$ and obtain the 90% C.L. exclusion limit on the electron-specific mediator coupling constant. Here we suppose that the signal originates from the MED-strahlung and e^+e^- annihilation mechanism, i. e. $N_{\rm sign} \simeq N^{\rm brem}_{\rm MED} + N^{\rm ann}_{\rm MED}$.

In the left panel (right panel) of Fig. 4 we show the experimental reach of the NA64 and LDMX for the electron-specific scalar (tensor) mediator coupling c^ϕ_{ee} ($c^{\rm G}_{ee}/\Lambda$). The expected limits associated with ϕ-strahlung (G-strahlung), $eN \to eN\phi(G)$, followed by invisible decay $\phi \to \chi\chi$ ($G \to \bar\psi\psi(SS)$) are depicted by the dashed-violet and dashed-orange lines for NA64 and LDMX, respectively. These expected reaches are derived for the projected statistics of NA64e at the level of EOT $\simeq 5 \times 10^{12}$ and for the LDMX with EOT $\simeq 10^{15}$. The existing limit of NA64 on c^ϕ_{ee} is shown by the solid-violet line, that implies EOT $\simeq 3.22 \times 10^{11}$.

For the projected statistics associated with positron annihilation mode we consider both positron and electron primary-beam options. In Fig. 4 the dashed pink and yellow lines correspond to the LDMX expected reach associated with electron and position beam, respectively.

It follows from Fig. 4 that the positron beam gives more stringent constraint on the mediator coupling constant due to the enhanced number of positron in the first generation of EM shower. In particular, for the LDMX mass range of interest $0.11\ {\rm GeV} \lesssim m_{\rm MED} \lesssim 0.13$ GeV the positron annihilation channel pushes down the exclusion limits by an order of magnitude. Note that the LDMX can reach a fairly strong limits on an electron-specific mediator due to the sufficiently large number of projected accumulated statistics

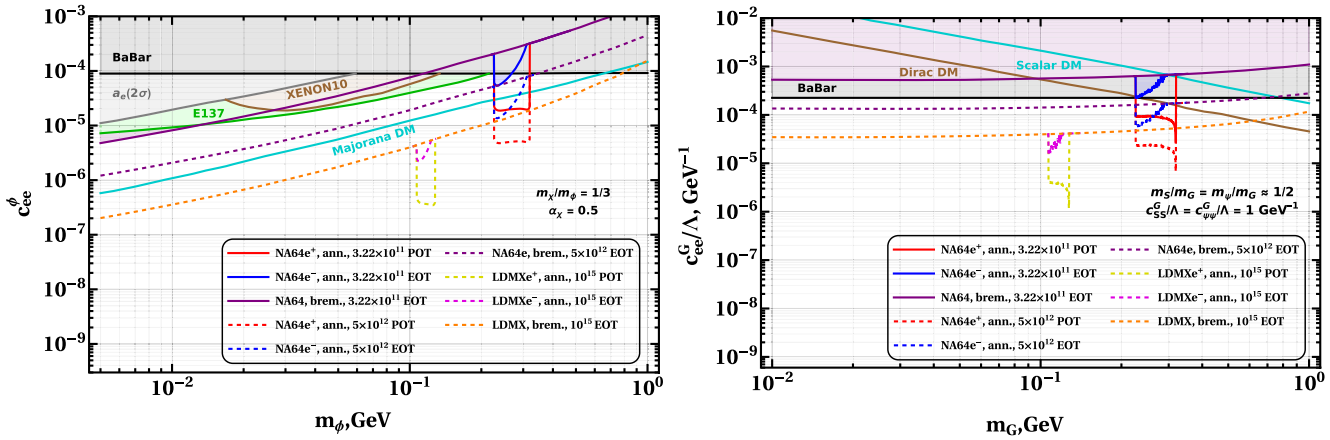

FIG. 4. Left panel: The experimental reach at 90% C.L. for the NA64 and LDMX fixed target facilities due to ϕ-strahlung and resonant positron annihilation $e^+e^- \to \phi$, followed by the invisible decay $\phi \to \chi\chi$. The solid-purple line corresponds to the existing NA64 limits for EOT $\simeq 3.22 \times 10^{11}$ from missing energy process $eN \to eN\phi$, the dashed-purple line shows the expected limit for projected statistics EOT $\simeq 5 \times 10^{12}$. The solid-blue line is the existing limit of the NA64 (EOT $\simeq 3.22 \times 10^{11}$) due to the positron annihilation mode $e^+e^- \to \phi$ with primary e^- beam, the solid-red line is the projected expected reach of NA64 for the positron annihilation channel with primary e^+ beam that corresponds to the 3.22×10^{11} positrons accumulated on target. Dashed blue and red lines correspond to the projected NA64 statistics 5×10^{12} of the annihilation mode $e^+e^- \to \phi$ for the e^- and e^+ primary beam, respectively. Dashed orange line is the projected LDMX limits for EOT $\simeq 10^{15}$ from ϕ-strahlung process $eN \to eN\phi$. Dashed pink and yellow lines correspond to the projected LDMX statistics 10^{15} of the annihilation mode $e^+e^- \to \phi$ for the e^- and e^+ primary beam respectively. Gray-shaded region corresponds to the exisiting *BABAR* [131] monophoton limit $e^+e^- \to \gamma\phi$. Green shaded region is the current reach of the electron-beam dump E137 [12,25,132] experiment. Brown-shaded region is the existing bound from XENON10 [133–135] direct detection experiment. Solid cyan line is the thermal targets for Majorana dark matter that couples to an electrophilic spin-0 mediator ϕ. The latter curve was adapted from top-left panel in Fig. 9 of Ref. [12], it implies the benchmark DM parameters $m_\chi/m_\phi = 1/3$ and $\alpha_\chi \simeq 0.5$. All these curves imply that mediator decays in the invisible mode, $\mathrm{Br}(\phi \to \chi\bar{\chi}) \simeq 1$. Right panel: The same as in the left plot but for the spin-2 mediator G. Shaded gray region corresponds to the current *BABAR* [34] monophoton $e^+e^- \to \gamma G$ reach. Solid brown and solid cyan lines corresponds to the thermal targets for Dirac DM and scalar DM that couple to an electrophilic spin-2 mediator G. These curves were adapted from left panel in Fig. 8 of Ref. [34], that implies the typical DM parameters $c_{SS}^{\mathrm{G}}/\Lambda = c_{\psi\psi}^{\mathrm{G}}/\Lambda \simeq 1.0$ GeV^{-1} and $m_S/m_G = m_\psi/m_G \simeq 0.498$. All these curves imply $\mathrm{Br}(G \to \psi\bar{\psi}) \simeq 1$ and $\mathrm{Br}(G \to SS) \simeq 1$. It is worth noticing again that for these benchmarks, the DM bounds are agnostic to the specific type of DM, i.e., the exclusion limits of scalar and Dirac DM from NA64 (LDMX) are indistinguishable (see text).

EOT $\simeq 10^{15}$. For instance, for the typical mass $m_\phi = m_G \simeq 0.1$ GeV the LDMX is able to set the constraint at the level of $c_{ee}^{\phi} \simeq 5 \times 10^{-7}$ and $c_{ee}^{\mathrm{G}}/\Lambda \simeq 10^{-6}$ GeV for the spin-0 and spin-2 mediator, respectively.

It is worth noticing that the authors of Ref. [12] have studied in detail the thermal production mechanism of DM involving parity-even electron-specific spin-0 mediator. In the left panel of Fig. 4 we show the relic-abundance target lines for Majorana DM by the solid-cyan line. That curve implies the benchmark DM parameters $m_\chi/m_\phi = 1/3$ and $\alpha_\chi \simeq 0.5$.

Remarkably, for the projected statistics EOT $\simeq 5 \times 10^{12}$ the NA64 facility can probe the thermal Majorana DM parameter space at the level of $c_{ee}^{\phi} \lesssim (3.0 - 4.0) \times 10^{-5}$ for the resonant channel $e^+e^- \to \chi\chi$ even with a primary electron-beam mode (dashed-blue line in left panel of Fig. 4). The significant enhancement of the sensitivity $c_{ee}^{\phi} \lesssim 5.0 \times 10^{-6}$ can be achieved by exploiting the positron beam mode of NA64 for the typical masses in the range 0.23 GeV $\lesssim m_{\mathrm{MED}} \lesssim 0.32$ GeV (dashed-red line in left panel of Fig. 4).

It is important to note, that the existing constraints of NA64 for EOT $\simeq 3.22 \times 10^{11}$ exceed the typical monophoton $e^+e^- \to \gamma\phi$ bound of the *BABAR* [131] facility at the level of $c_{ee}^{\phi} \lesssim 6 \times 10^{-5}$. Moreover, the current limits of NA64 associated with ϕ-strahlung are complementary to the experimental reach of the E137 [12,25,132] and XENON10 [133–135] direct-detection experiment for $m_\phi \lesssim 10^{-2}$ GeV and $c_{ee}^{\phi} \lesssim 10^{-5}$.

In addition we note that the thermal production mechanism of DM involving spin-2 electrophilic mediator have been analyzed in detail in Ref. [34]. To be more specific, in right panel of Fig. 4 we show the typical relic-abundance target curves for the scalar (solid cyan line) and Dirac DM (solid brown line) adapted from Ref. [34]. These lines imply the typical DM couplings $c_{SS}^{\mathrm{G}}/\Lambda = c_{\psi\psi}^{\mathrm{G}}/\Lambda \simeq 1.0$ GeV^{-1} and benchmark mass ratios that are close to the DM production threshold $m_S/m_G = m_\psi/m_G \simeq 0.498$.

This means that one can use the approximate Eq. (24) in the calculation of the yield of the spin-2 mediator, as long as $\Gamma_G \to 0$ for $m_G \simeq 2m_{\rm DM}$. It is worth noticing again that for these benchmarks, the DM bounds of an electron fixed target are agnostic to the specific type of DM, i.e., the exclusion limits of scalar and Dirac DM are indistinguishable.

The bound from invisible monophoton searches $e^+e^- \to \gamma G$ at *BABAR* applies to the typical parameter space of the spin-2 mediator with $m_G \lesssim 1$ GeV and $c^{\rm G}_{ee}/\Lambda \lesssim 2 \times 10^{-4}$ GeV^{-1}. This bound rules out the existing G-strahlung constraints from NA64 for EOT $\simeq 3.22 \times 10^{11}$. However, the resonant mechanism of DM production with NA64 (solid-blue line in right panel of Fig. 4) provides the bound on $c^{\rm G}_{ee}/\Lambda$ that barely touches the *BABAR* limit at $m_G \simeq 0.23$ GeV. Remarkably, the latter constraint is associated also with Dirac DM relic curve. However, the scalar DM is almost ruled out by *BABAR*. We note that for the projected statistics EOT $\simeq 5 \times 10^{12}$ of NA64 one can probe the Dirac DM at the level of $c^{\rm G}_{ee}/\Lambda \lesssim 2.0 \times 10^{-4}$ GeV^{-1} for $m_G \simeq 0.3$ GeV. Finally, we note that positron beam mode exploiting in the NA64 (with $\simeq 5 \times 10^{12}$ positrons accumulated on target) can set a fairly strong bound at $c^{\rm G}_{ee}/\Lambda \lesssim 10^{-5}$ GeV^{-1} that is complementary to the LDMX expected reach for EOT $\simeq 10^{15}$ at $m_G \simeq 3 \times 10^{-1}$ GeV. However, the latter facility can rule out the spin-2 parameter space $c^{\rm G}_{ee}/\Lambda \lesssim 1 \times 10^{-6}$ GeV^{-1} in the resonant mode close to typical mass at $m_G \simeq 1.5 \times 10^{-1}$ GeV.

VIII. CONCLUSION

In the present paper we have studied in detail the resonant probing spin-0 and spin-2 DM mediator with electron fixed target experiments NA64 and LDMX. In particular, we showed that e^+ resonant annihilation $e^+e^- \to {\rm MED} \to {\rm DM} + {\rm DM}$ can be a viable mechanism of the electron-specific DM mediator production, such that this process is competitive with widely exploited MED-strahlung production, $eN \to eN$ MED, followed by the invisible decay into pair of DM particles, MED $\to$ DM + DM. Moreover, we estimated the reach of NA64 and LDMX and showed that the exclusion limits are pushed down by factor of $\mathcal{O}(1)$ for the specific mass range of the mediators.

ACKNOWLEDGMENTS

We would like to thank A. Celentano, P. Crivelli, S. Demidov, R. Dusaev, S. Gninenko, D. Gorbunov, M. Kirsanov, N. Krasnikov, V. Lyubovitskij, L. Molina Bueno, A. Pukhov, H. Sieber, and A. Zhevlakov for very helpful discussions and correspondences. The work of D. V. K on description of the dark matter missing energy signatures of NA64e and exclusion limits for spin-2 DM mediator is supported by the Russian Science Foundation RSF Grant No. 21-12-00379.

APPENDIX: MAJORANA FERMION

In this section we calculate a width of decay and a resonant cross section for the spin-0 mediator with Majorana fermions in a final state. For calculations below, we use two-component spinors formalism from [122].

The Lagrangian of interaction between spin-0 massive mediator ϕ and Majorana fermions χ is

$$\mathcal{L}^{\phi}_{\rm Majorana} \supset -\frac{1}{2} c^{\phi}_{\chi\chi} \phi\chi\chi + \frac{1}{2} m_\chi \chi\chi + {\rm H.c.} \tag{A1}$$

The matrix element for a decay of spin-0 mediator ϕ into pair of Majorana fermions $\phi(p,s) \to \chi(p_1,s_1)\chi(p_2,s_2)$ takes the following form [122]:

$$iM = -ic^{\phi}_{\chi\chi}(y_1 y_2 + x_1^\dagger x_2^\dagger), \tag{A2}$$

where the two-component spinors are

$$x_i{}^\alpha = x^\alpha(\boldsymbol{p}_i, s_i), \qquad y_i{}^\alpha = y^\alpha(\boldsymbol{p}_i, s_i).$$

The summation over spinor indices is defined as $y_1{}^\alpha \delta_\alpha{}^\beta y_{2\beta} = y_1 y_2$. Moreover we imply the notation $x^\alpha y_\alpha$ and $x_{\dot\alpha} y^{\dot\alpha}$, where the undotted and dotted indices correspond to the left-handed and right-handed fermions, respectively, they are related via the Hermitian conjugation.

Also, for a raising and a lowering indices we use the antisymmetric tensor 2×2 that has the following form:

$$\epsilon^{12} = -\epsilon_{12} = 1, \qquad \epsilon_{\alpha\beta}\epsilon^{\gamma\delta} = \delta^\delta_\alpha \delta^\gamma_\beta - \delta^\gamma_\alpha \delta^\delta_\beta.$$

The (anti)commutation relations read [136]

$$xy = x^\alpha y_\alpha = -x_\alpha y^\alpha = y^\alpha x_\alpha = yx, \qquad xy = -yx.$$

By taking into account the spin sum [122], we get expressions in the following form:

$$\begin{aligned}
\sum_{\rm spins}(y_1 y_2)(y_2^\dagger y_1^\dagger) &= \sum_{\rm spins} \delta_\alpha{}^\beta \delta_{\dot\gamma}{}^{\dot\lambda} y_1{}^\alpha y_{2\beta} y^\dagger_{2\dot\lambda} y_1^{\dagger\dot\gamma} \\
&= (p_2, \sigma_{\beta\dot\lambda})(p_1, \bar\sigma^{\dot\lambda\beta}) = p_2{}^\mu p_1{}^\nu {\rm Tr}(\sigma_\mu \bar\sigma_\nu) \\
&= 2(p_1, p_2), \\
\sum_{\rm spins} x_1^\dagger x_2^\dagger y_2^\dagger y_1^\dagger &= \sum_{\rm spins} \delta_{\dot\alpha}{}^{\dot\beta} \delta_{\dot\gamma}{}^{\dot\lambda} x^\dagger_{1\dot\beta} x_2^{\dagger\dot\alpha} y^\dagger_{2\dot\lambda} y_1^{\dagger\dot\gamma} \\
&= -m_\chi^2 \delta_\alpha{}^{\dot\beta} \delta_{\dot\gamma}{}^{\dot\lambda} \delta_{\dot\lambda}{}^{\dot\alpha} \delta_{\dot\beta}{}^{\dot\gamma} = -m^2 \delta_{\dot\beta}{}^{\dot\beta} = -2m_\chi^2, \\
\sum_{\rm spins} y_1 y_2 x_2 x_1 &= -2m_\chi^2, \qquad \sum_{\rm spins} x_1^\dagger x_2^\dagger x_2 x_1 = 2(p_1, p_2),
\end{aligned}$$

where $\sigma^\mu = (\mathbb{I}_{2\times 2}, \boldsymbol{\sigma})$, $\bar\sigma^\mu = (\mathbb{I}_{2\times 2}, -\boldsymbol{\sigma})$ with $\boldsymbol{\sigma}$ being a matrices of Pauli. Finally, the matrix element squared by assuming the summation over the final states is

$$\sum_{\text{spins}} |M|^2 = 4(c^{\phi}_{\chi\chi})^2[(p_1, p_2) - m_\chi^2]. \tag{A3}$$

The decay width can be written as follows:

$$\Gamma_{\phi\to\chi\chi} = \frac{1}{2}\cdot\frac{1}{16\pi m_\phi^3}\lambda^{1/2}(m_\phi^2, m_\chi^2, m_\chi^2)\sum_{\text{spins}}|M|^2, \tag{A4}$$

where $\lambda(x, y, y) = x^2(1 - 4y/x)$ is the triangle function, the extra factor of $1/2$ in Eq. (A4) is due to the identical Majorana particles in the final state [122]. As a result one has

$$\Gamma_{\phi\to\chi\chi} = \frac{1}{4}\alpha_\chi m_\phi(1 - 4m_\chi^2/m_\phi^2)^{3/2}. \tag{A5}$$

The cross section reads

$$\sigma_{e^-e^+\to\phi\to\chi\chi} = \frac{1}{2}\cdot\frac{4\pi\alpha_\chi(c^{\phi}_{ee})^2}{16\pi}\frac{s\left(1-\frac{4m_\chi^2}{s}\right)^{3/2}}{(s-m_\phi^2)^2 + m_\phi^2\Gamma_\phi^2}. \tag{A6}$$

[1] P. A. R. Ade *et al.* (Planck Collaboration), Astron. Astrophys. **594**, A13 (2016).
[2] N. Aghanim *et al.* (Planck Collaboration), Astron. Astrophys. **641**, A6 (2020); **652**, C4(E) (2021).
[3] G. Bertone, D. Hooper, and J. Silk, Phys. Rep. **405**, 279 (2005).
[4] L. Bergstrom, Ann. Phys. (Berlin) **524**, 479 (2012).
[5] G. B. Gelmini, in *Journeys Through the Precision Frontier: Amplitudes for Colliders* (World Scientific, Singapore, 2015), pp. 559–616.
[6] B. W. Lee and S. Weinberg, Phys. Rev. Lett. **39**, 165 (1977).
[7] C. Boehm, T. A. Ensslin, and J. Silk, J. Phys. G **30**, 279 (2004).
[8] C. Boehm and P. Fayet, Nucl. Phys. **B683**, 219 (2004).
[9] M. Pospelov, A. Ritz, and M. B. Voloshin, Phys. Lett. B **662**, 53 (2008).
[10] N. Arkani-Hamed, D. P. Finkbeiner, T. R. Slatyer, and N. Weiner, Phys. Rev. D **79**, 015014 (2009).
[11] G. Krnjaic, Phys. Rev. D **94**, 073009 (2016).
[12] A. Berlin, N. Blinov, G. Krnjaic, P. Schuster, and N. Toro, Phys. Rev. D **99**, 075001 (2019).
[13] J. McDonald, Phys. Rev. D **50**, 3637 (1994).
[14] C. P. Burgess, M. Pospelov, and T. ter Veldhuis, Nucl. Phys. **B619**, 709 (2001).
[15] J. D. Wells, arXiv:0803.1243.
[16] R. M. Schabinger and J. D. Wells, Phys. Rev. D **72**, 093007 (2005).
[17] G. Bickendorf and M. Drees, Eur. Phys. J. C **82**, 1163 (2022).
[18] E. E. Boos, V. E. Bunichev, and S. S. Trykov, Phys. Rev. D **107**, 075021 (2023).
[19] H. Sieber, D. V. Kirpichnikov, I. V. Voronchikhin, P. Crivelli, S. N. Gninenko, M. M. Kirsanov, N. V. Krasnikov, L. Molina-Bueno, and S. Sekatskii, arXiv:2305.09015.
[20] B. Holdom, Phys. Lett. **166B**, 196 (1986).
[21] L. B. Okun, Sov. Phys. JETP **56**, 502 (1982), http://jetp.ras.ru/cgi-bin/e/index/e/56/3/p502?a=list.
[22] E. Izaguirre, G. Krnjaic, P. Schuster, and N. Toro, Phys. Rev. Lett. **115**, 251301 (2015).
[23] R. Essig, P. Schuster, N. Toro, and B. Wojtsekhowski, J. High Energy Phys. 02 (2011) 009.
[24] Y. Kahn, G. Krnjaic, J. Thaler, and M. Toups, Phys. Rev. D **91**, 055006 (2015).
[25] B. Batell, R. Essig, and Z. Surujon, Phys. Rev. Lett. **113**, 171802 (2014).
[26] B. Batell, A. Freitas, A. Ismail, and D. Mckeen, Phys. Rev. D **98**, 055026 (2018).
[27] E. Izaguirre, G. Krnjaic, P. Schuster, and N. Toro, Phys. Rev. D **88**, 114015 (2013).
[28] A. Kachanovich, S. Kovalenko, S. Kuleshov, V. E. Lyubovitskij, and A. S. Zhevlakov, Phys. Rev. D **105**, 075004 (2022).
[29] V. E. Lyubovitskij, A. S. Zhevlakov, A. Kachanovich, and S. Kuleshov, Phys. Rev. D **107**, 055006 (2023).
[30] D. Gorbunov and D. Kalashnikov, Phys. Rev. D **107**, 015014 (2023).
[31] J. Claude, M. Dutra, and S. Godfrey, Phys. Rev. D **107**, 075006 (2023).
[32] W. Wang, W.-L. Xu, J. M. Yang, and R. Zhu, arXiv:2305.12668.
[33] H. M. Lee, M. Park, and V. Sanz, Eur. Phys. J. C **74**, 2715 (2014).
[34] Y.-J. Kang and H. M. Lee, Eur. Phys. J. C **80**, 602 (2020).
[35] N. Bernal, M. Dutra, Y. Mambrini, K. Olive, M. Peloso, and M. Pierre, Phys. Rev. D **97**, 115020 (2018).
[36] M. G. Folgado, A. Donini, and N. Rius, J. High Energy Phys. 04 (2020) 036.
[37] Y.-J. Kang and H. M. Lee, Eur. Phys. J. C **81**, 868 (2021).
[38] M. Dutra, *Proc. Sci.* LeptonPhoton2019 (2019) 076.
[39] S. Clery, Y. Mambrini, K. A. Olive, A. Shkerin, and S. Verner, Phys. Rev. D **105**, 095042 (2022).
[40] H. M. Lee, M. Park, and V. Sanz, J. High Energy Phys. 05 (2014) 063.
[41] J. A. Gill, D. Sengupta, A. G, and Williams, arXiv:2303.04329.
[42] W. Wang, L. Wu, J. M. Yang, H. Zhou, and B. Zhu, J. High Energy Phys. 12 (2020) 072; 02 (2021) 52.
[43] A. de Giorgi and S. Vogl, J. High Energy Phys. 11 (2021) 036.

[44] A. de Giorgi and S. Vogl, J. High Energy Phys. 04 (2023) 032.
[45] K. Jodłowski, arXiv:2305.05710.
[46] G. N. Wojcik, L. L. Everett, S. T. Eu, and R. Ximenes, arXiv:2303.12983.
[47] A. Jueid and S. Nasri, arXiv:2301.12524.
[48] J. Kawamura, S. Okawa, and Y. Omura, Phys. Rev. D **106**, 015005 (2022).
[49] Y. Bai and J. Berger, J. High Energy Phys. 08 (2014) 153.
[50] J. Kawamura, S. Okawa, and Y. Omura, J. High Energy Phys. 08 (2020) 042.
[51] Z. Xu, R. Zhang, and S. Zheng, arXiv:2304.02904.
[52] B. Shakya, Mod. Phys. Lett. A **31**, 1630005 (2016).
[53] O. Lebedev and T. Toma, J. High Energy Phys. 05 (2023) 108.
[54] A. Poulin, Phys. Rev. D **100**, 043022 (2019).
[55] K. R. Dienes, D. Kim, H. Song, S. Su, B. Thomas, and D. Yaylali, Phys. Rev. D **101**, 075024 (2020).
[56] M. Bauer, P. Foldenauer, P. Reimitz, and T. Plehn, SciPost Phys. **10**, 030 (2021).
[57] A. Poulin and S. Godfrey, Phys. Rev. D **99**, 076008 (2019).
[58] J. L. Feng *et al.*, J. Phys. G **50**, 030501 (2023).
[59] G. Krnjaic *et al.*, arXiv:2207.00597.
[60] S. Gori *et al.*, arXiv:2209.04671.
[61] P. Crivelli, Status and prospects of the NA64 experiment at the CERN SPS, arXiv:2301.09905.
[62] P. Agrawal *et al.*, Eur. Phys. J. C **81**, 1015 (2021).
[63] K. Bondarenko, A. Boyarsky, O. Mikulenko, R. Jacobsson, and M. Ovchynnikov, arXiv:2304.02511.
[64] G. Lanfranchi, J. Phys. Conf. Ser. **1526**, 012029 (2020).
[65] G. Lanfranchi, M. Pospelov, and P. Schuster, Annu. Rev. Nucl. Part. Sci. **71**, 279 (2021).
[66] P. J. Fox *et al.*, arXiv:2210.03075.
[67] S. N. Gninenko, N. V. Krasnikov, M. M. Kirsanov, and D. V. Kirpichnikov, Phys. Rev. D **94**, 095025 (2016).
[68] D. Banerjee *et al.* (NA64 Collaboration), Phys. Rev. Lett. **118**, 011802 (2017).
[69] D. Banerjee *et al.* (NA64 Collaboration), Phys. Rev. D **97**, 072002 (2018).
[70] S. N. Gninenko, D. V. Kirpichnikov, M. M. Kirsanov, and N. V. Krasnikov, Phys. Lett. B **782**, 406 (2018).
[71] D. Banerjee *et al.* (NA64 Collaboration), Phys. Rev. Lett. **120**, 231802 (2018).
[72] S. N. Gninenko, D. V. Kirpichnikov, and N. V. Krasnikov, Phys. Rev. D **100**, 035003 (2019).
[73] S. N. Gninenko, D. V. Kirpichnikov, M. M. Kirsanov, and N. V. Krasnikov, Phys. Lett. B **796**, 117 (2019).
[74] D. Banerjee *et al.*, Phys. Rev. Lett. **123**, 121801 (2019).
[75] D. Banerjee *et al.* (NA64 Collaboration), Phys. Rev. D **101**, 071101 (2020).
[76] R. R. Dusaev, D. V. Kirpichnikov, and M. M. Kirsanov, Phys. Rev. D **102**, 055018 (2020).
[77] D. Banerjee *et al.* (NA64 Collaboration), Phys. Rev. Lett. **125**, 081801 (2020).
[78] E. Depero *et al.* (NA64 Collaboration), Eur. Phys. J. C **80**, 1159 (2020).
[79] M. Bondi, A. Celentano, R. R. Dusaev, D. V. Kirpichnikov, M. M. Kirsanov, N. V. Krasnikov, L. Marsicano, and D. Shchukin, Comput. Phys. Commun. **269**, 108129 (2021).
[80] Y. M. Andreev *et al.* (NA64 Collaboration), Phys. Rev. Lett. **126**, 211802 (2021).
[81] Y. M. Andreev *et al.* (NA64 Collaboration), Phys. Rev. D **104**, L111102 (2021).
[82] C. Cazzaniga *et al.* (NA64 Collaboration), Eur. Phys. J. C **81**, 959 (2021).
[83] Y. M. Andreev *et al.*, Phys. Rev. D **104**, L091701 (2021).
[84] Y. M. Andreev *et al.* (NA64 Collaboration), Phys. Rev. D **106**, 032015 (2022).
[85] N. Arefyeva, S. Gninenko, D. Gorbunov, and D. Kirpichnikov, Phys. Rev. D **106**, 035029 (2022).
[86] A. S. Zhevlakov, D. V. Kirpichnikov, and V. E. Lyubovitskij, Phys. Rev. D **106**, 035018 (2022).
[87] I. V. Voronchikhin and D. V. Kirpichnikov, Phys. Rev. D **106**, 115041 (2022).
[88] M. Mongillo, A. Abdullahi, B. B. Oberhauser, P. Crivelli, M. Hostert, D. Massaro, L. M. Bueno, and S. Pascoli, Eur. Phys. J. C **83**, 391 (2023),
[89] A. M. Abdullahi, M. Hostert, D. Massaro, and S. Pascoli, arXiv:2302.05410.
[90] J. Mans (LDMX Collaboration), EPJ Web Conf. **142**, 01020 (2017).
[91] T. Åkesson *et al.*, in Snowmass 2021 (2022), arXiv:2203.08192.
[92] B. Echenard, Astrophys. Space Sci. Proc. **56**, 49 (2019).
[93] O. Moreno (LDMX Collaboration), Proc. Sci. ICHEP2018 (**2019**) 395.
[94] A. M. Ankowski, A. Friedland, S. W. Li, O. Moreno, P. Schuster, N. Toro, and N. Tran, Phys. Rev. D **101**, 053004 (2020).
[95] L. K. Bryngemark *et al.*, EPJ Web Conf. **251**, 02038 (2021).
[96] P. Schuster, N. Toro, and K. Zhou, Phys. Rev. D **105**, 035036 (2022).
[97] L. Marsicano, M. Battaglieri, M. Bondí, C. D. R. Carvajal, A. Celentano, M. De Napoli, R. De Vita, E. Nardi, M. Raggi, and P. Valente, Phys. Rev. Lett. **121**, 041802 (2018).
[98] L. Marsicano, M. Battaglieri, M. Bondi', C. D. R. Carvajal, A. Celentano, M. De Napoli, R. De Vita, E. Nardi, M. Raggi, and P. Valente, Phys. Rev. D **98**, 015031 (2018).
[99] A. Celentano, L. Darmé, L. Marsicano, and E. Nardi, Phys. Rev. D **102**, 075026 (2020).
[100] M. Battaglieri *et al.*, Eur. Phys. J. A **57**, 253 (2021).
[101] D. Forbes, C. Herwig, Y. Kahn, G. Krnjaic, C. Mantilla Suarez, N. Tran, and A. Whitbeck, arXiv:2212.00033.
[102] C.-Y. Chen, J. Kozaczuk, and Y.-M. Zhong, J. High Energy Phys. 10 (2018) 154.
[103] L. Marsicano, M. Battaglieri, A. Celentano, R. De Vita, and Y.-M. Zhong, Phys. Rev. D **98**, 115022 (2018).
[104] B. Batell, N. Lange, D. McKeen, M. Pospelov, and A. Ritz, Phys. Rev. D **95**, 075003 (2017).
[105] C.-Y. Chen, H. Davoudiasl, W. J. Marciano, and C. Zhang, Phys. Rev. D **93**, 035006 (2016).
[106] M. Nemevšek, F. Nesti, and J. C. Vasquez, J. High Energy Phys. 04 (2017) 114.
[107] Y.-S. Liu, D. McKeen, and G. A. Miller, Phys. Rev. D **95**, 036010 (2017).
[108] Y.-S. Liu and G. A. Miller, Phys. Rev. D **96**, 016004 (2017).

[109] D. V. Kirpichnikov, H. Sieber, L. M. Bueno, P. Crivelli, and M. M. Kirsanov, Phys. Rev. D **104**, 076012 (2021).
[110] H. Sieber, D. Banerjee, P. Crivelli, E. Depero, S. N. Gninenko, D. V. Kirpichnikov, M. M. Kirsanov, V. Poliakov, and L. Molina Bueno, Phys. Rev. D **105**, 052006 (2022).
[111] J. D. Bjorken, R. Essig, P. Schuster, and N. Toro, Phys. Rev. D **80**, 075018 (2009).
[112] L. Darmé, F. Giacchino, E. Nardi, and M. Raggi, J. High Energy Phys. 06 (2021) 009.
[113] J. Liang, Z. Liu, and L. Yang, J. High Energy Phys. 05 (2022) 184.
[114] J. Liu, Y. Luo, and M. Song, arXiv:2304.05435.
[115] Y.-Z. Chen, Y.-A. Luo, L. Li, H. Shen, and X.-Q. Li, Commun. Theor. Phys. **55**, 1059 (2011).
[116] J. D. Lewin and P. F. Smith, Astropart. Phys. **6**, 87 (1996).
[117] B. Döbrich, J. Jaeckel, F. Kahlhoefer, A. Ringwald, and K. Schmidt-Hoberg, J. High Energy Phys. 02 (2016) 018.
[118] K. Freese, J. A. Frieman, and A. Gould, Phys. Rev. D **37**, 3388 (1988).
[119] V. Shtabovenko, R. Mertig, and F. Orellana, Comput. Phys. Commun. **256**, 107478 (2020).
[120] V. Shtabovenko, R. Mertig, and F. Orellana, Comput. Phys. Commun. **207**, 432 (2016).
[121] W. R. Inc., Mathematica, Version 13.1, Champaign, IL, 2022.
[122] H. K. Dreiner, H. E. Haber, and S. P. Martin, Phys. Rep. **494**, 1 (2010).
[123] H. Bethe and W. Heitler, Proc. R. Soc. A **146**, 83 (1934).
[124] J. F. Carlson and J. R. Oppenheimer, Phys. Rev. **51**, 220 (1937).
[125] L. D. Landau, Proc. R. Soc. A **166**, 252 (1938).
[126] Y.-S. Tsai and V. Whitis, Phys. Rev. **149**, 1248 (1966).
[127] We would like to thank Andrea Celentano for sharing the code and numerical data of Fig. 2.
[128] S. Agostinelli *et al.* (GEANT4 Collaboration), Nucl. Instrum. Methods Phys. Res., Sect. A **506**, 250 (2003).
[129] Y. M. Andreev *et al.* (NA64 Collaboration), Phys. Rev. Lett. **129**, 161801 (2022).
[130] T. Åkesson *et al.* (LDMX Collaboration), J. High Energy Phys. 04 (2020) 003.
[131] J. P. Lees *et al.* (*BABAR* Collaboration), Phys. Rev. Lett. **119**, 131804 (2017).
[132] J. D. Bjorken, S. Ecklund, W. R. Nelson, A. Abashian, C. Church, B. Lu, L. W. Mo, T. A. Nunamaker, and P. Rassmann, Phys. Rev. D **38**, 3375 (1988).
[133] J. Angle *et al.* (XENON10 Collaboration), Phys. Rev. Lett. **107**, 051301 (2011); **110**, 249901(E) (2013).
[134] R. Essig, A. Manalaysay, J. Mardon, P. Sorensen, and T. Volansky, Phys. Rev. Lett. **109**, 021301 (2012).
[135] R. Essig, T. Volansky, and T.-T. Yu, Phys. Rev. D **96**, 043017 (2017).
[136] M. D. Schwartz, *Quantum Field Theory and the Standard Model* (Cambridge University Press, Cambridge, England, 2014).